ELSEVIER

International Journal of Heat and Fluid Flow 20 (1999) 499–506

International Journal of HEAT AND FLUID FLOW

www.elsevier.com/locate/ijhff

Influence of the viscosity on the linear stability of an annular liquid sheet

Xavier Jeandel, Christophe Dumouchel *

Laboratoire de Thermodynamique, CORIA–UMR 6614, Université et INSA de Rouen, 76821 Mont-Saint-Aignan, Cedex, France

Abstract

This paper reports a study of the linear stability of an annular liquid sheet evolving in a gaseous environment at rest. In this investigation, the viscosity of the liquid is taken into account. As has been found in similar approaches developed for other liquid systems, the results reveal the presence of a dominant wave and a cut-off wave number for each set of initial conditions. A complete parametric study is conducted. This shows a very specific influence of the surface tension due to the presence of the natural curvature of the liquid system. It also shows that the influence of the liquid viscosity is stabilising, and that the importance of the action of these forces is a function of the other parameters. A non-dimensional number D is derived from this study. This number, consistent with that derived for flat liquid systems in a previous investigation, allows one to account for the influence of the liquid viscosity on the linear stability of an annular liquid sheet. © 1999 Elsevier Science Inc. All rights reserved.

Notation

a	internal radius of the annular liquid sheet
h	liquid sheet thickness
k	wave-number
k_c	cutt-off wave-number
k_{opt}	dominant wave wave-number
p	pressure
r	radial position
Re	Reynolds number ($=\rho_L Uh/\mu$)
t	time
U	relative velocity
(u, v)	perturbation velocity component
x	axial position
ϕ	perturbation potential function
ψ	liquid stream function
η^*	interface displacement function
η_0^*	amplitude of the perturbation
μ	dynamic liquid viscosity
ν	kinematic liquid viscosity
θ	azimuthal angle
ρ_G, ρ_L	gas and liquid density
σ	surface tension
ω	complex frequency ($=\omega_r + i\omega_i$)
ω_i	growth rate
ω_{imax}	dominant wave growth rate
Subscript	
i	interface
j	phase flow

1. Introduction

Theoretical investigations on liquid atomisation and spray formation are very much required in order to help in the improvement of injection systems on the basis of theoretical considerations rather than on time consuming and expensive experimental tests. The development of theoretical approaches dedicated to spray formation is complicated by the fact that the physics of atomisation is only partially known at present. Basic models are therefore still appreciated as they are regarded as a first step to the development of more complete theoretical approaches. Furthermore, they can provide some indications on the main parameters that influence the process in a given situation as well as the nature of this influence. Although in many cases this information is qualitative, it can help in defining a strategy for improving a given injection system.

The linear theory is probably the best-known basic approach. It has been developed for many different liquid systems such as plain cylindrical jets (Rayleigh, 1879, Weber, 1931, Sterling and Sleicher, 1975) and liquid sheets whether flat (Squire, 1953, Chigier and Dumouchel, 1996, Cousin and Dumouchel, 1996), radial (Weihs, 1978) or annular (Crapper et al., 1975, Lee and Chen, 1991, Dumouchel and Ledoux, 1991). The linear theory shows multiple advantages. It is based on quite simple considerations, and the mathematical requirements are not too severe. Furthermore, in many situations, it has been found that the linear theory allows one to determine an instability criterion (Rayleigh, 1879, Squire, 1953) and to calculate a characteristic length scale of the atomisation process studied. When a scheme of disintegration is defined, this characteristic length scale leads to the determination of a theoretical drop diameter. In some situations, this calculated diameter is satisfactorily representative of the drop-size distribution (Dumouchel et al., 1990). In any event, it

* Corresponding author. E-mail: christophe.dumouchel@coria.fr

0142-727X/99/$ – see front matter © 1999 Elsevier Science Inc. All rights reserved.
PII: S0142-727X(99)00038-7

always shows dependence on the main parameters in agreement with the experimentally observed trends.

In the present study, the linear theory is applied on an annular liquid sheet evolving in a gaseous environment at rest. The formation of sprays through the disintegration of such a liquid system corresponds to several industrial applications. Furthermore, the study of the annular liquid sheet can be regarded as being the first step towards the more complex problem of a conical liquid system (Dumouchel et al., 1990). The main purpose is here to investigate the influence of the liquid viscosity to see in which conditions this physical property influences the atomisation process. The approach developed can be regarded as an extension of the study on the flat viscous liquid sheet reported in a previous paper (Cousin and Dumouchel, 1996).

2. Mathematical considerations

The linear theory is developed for an annular liquid sheet defined by a thickness h and an inner radius a as shown in Fig. 1. For convenience the problem is set in a cylindrical coordinate system (x, r, θ) moving with the liquid. The following assumptions are made: both fluids are assumed incompressible, the viscosity of the gas is not taken into account, and the thickness of the liquid sheet is assumed to be constant. Moreover, in order to suppress the non-linear terms in the equations, the amplitude of the perturbation is assumed to be very small compared to its wavelength λ and to the sheet thickness h. Both interfaces are perturbed by a sinusoidal disturbance defined by a wave number k. This disturbance induces a displacement of the outer and the inner interfaces that is introduced by the function η_i defined by:

$$\eta_i = \eta_{0i}\exp[\mathrm{i}(kx - \omega t)], \tag{1}$$

where i ($=1$, 2) refers to the outer and inner interface respectively (Fig. 1). The initial flow is steady and the presence of the perturbation induces a non-steady flow in both fluids. The pressure and the velocity are written as the sum of a mean and a disturbed part corresponding to the steady and unsteady flows respectively. The purpose of the calculation is to determine the frequency ω for any sinusoidal perturbation defined by a wave number k. The frequency ω may be complex. According to Eq. (1), a complex solution with a positive imaginary part ω_i, indicates that the imposed perturbation will grow and ω_i represents the growth rate of this perturbation.

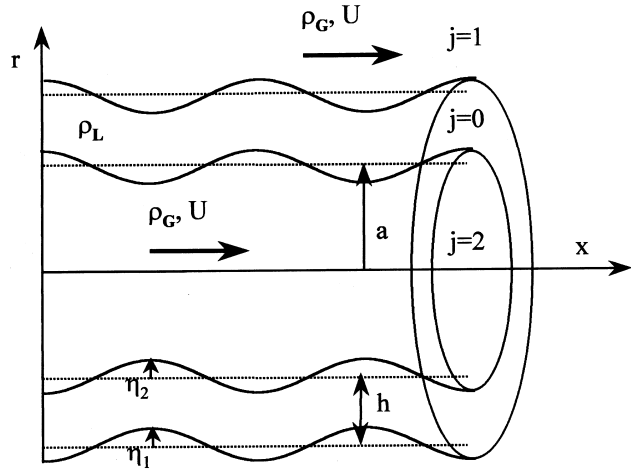

Fig. 1. Description of the annular liquid sheet.

Following the classical linear theory development and according to the assumptions the disturbed part of the velocity in each fluid is associated to a potential function ϕ. As the liquid viscosity is taken into account, the potential function in this fluid is completed by a stream function ψ. Thus, the disturbed velocities are given by:

$$\vec{v_j} = \vec{\mathrm{grad}}\phi_j \quad j = 1,2 \tag{2}$$

for the gas perturbation flows, and by:

$$\vec{v_0} = \vec{\mathrm{grad}}\phi_0 + \vec{\mathrm{rot}}\,\vec{A}, \tag{3}$$

where $\vec{A} = (0,0,\psi/r)$ for the liquid flow. The fluid dynamic equations are written in both fluids. In the liquid as well as in the outer and inner gas, the continuity equation with Eqs. (2) and (3) yields:

$$\Delta\phi_j = 0 \quad j = 0,1,2. \tag{4}$$

These three equations allow one to find the mathematical form for the potential functions. The form is:

$$\phi_j = \left[B_jI_0(kr) + C_jK_0(kr)\right]\exp[\mathrm{i}(kx - \omega t)] \quad j = 0,1,2, \tag{5}$$

where B_j and C_j are unknowns to be determined and I_0 and K_0 are modified Bessel functions classically encountered in axisymmetric problems. Using Eq. (3), the momentum equation in the liquid takes the following form:

$$\vec{\mathrm{grad}}\left(\frac{\mathrm{d}\phi_0}{\mathrm{d}t} + \frac{p_0}{\rho_\mathrm{L}}\right) = \vec{\mathrm{rot}}\left(\nu\Delta\vec{A} - \frac{\mathrm{d}\vec{A}}{\mathrm{d}t}\right). \tag{6}$$

By applying the curl, Eq. (6) reduces to an equation from which the stream function is determined, namely

$$\psi = r[DI_1(k_1r) + EK_1(k_1r)]\exp[\mathrm{i}(kx - \omega t)], \tag{7}$$

where $k_1^2 = k^2 - \mathrm{i}\omega/\nu$, D and E are two other unknowns to be calculated, and I_1 and K_1 are modified Bessel functions. At this stage, for a given perturbation wave number k, the calculation of the frequency ω requires the determination of 10 unknowns, namely, B_0, C_0, B_1, C_1, B_2, C_2, D, E, η_{01} and η_{02}. To achieve this, conditions are written on each interface. First, the kinematic conditions express the fact that the interfaces always comprise the same fluid particles:

$$\begin{aligned} v_i &= \frac{\partial\eta_i}{\mathrm{d}t} + U\frac{\partial\eta_i}{\partial x}, \\ v_0 &= \frac{\partial\eta_i}{\partial t} \quad i = 1,2. \end{aligned} \tag{8}$$

The system of Eq. (8) is completed by the dynamic conditions expressing the continuity of the stress tensor components across each interface. Two equations are then written at each interface:

$$\begin{aligned} &\frac{\partial u_0}{\partial r} + \frac{\partial v_0}{\partial x} = 0, \\ &-p_0 + 2\mu\frac{\partial v_0}{\partial r} = -p_i + p_{\sigma i} \quad i = 1,2, \end{aligned} \tag{9}$$

where the contribution of the surface tension is given by

$$p_{\sigma i} = \sigma\left(\frac{\eta_i}{r^2} + \frac{\partial^2\eta_i}{\partial x^2}\right) \quad i = 1,2. \tag{10}$$

The eight unknowns contained in the three potential functions and in the liquid stream function can be calculated using the four Eqs. (8), the conservation of the tangential component of the stress tensor through each interface (the first equation of system (9)), and the boundary conditions when $r \to 0$ and $r \to \infty$. The problem reduces then to a system of two equations

with two unknowns. The two equations express the conservation of the normal component of the stress tensor through each interface (the second equation of system (9)) and the two unknowns are the initial amplitude of the perturbation on each interface. This system is given by

$$\begin{aligned}
&\frac{(2-\Omega)^2}{Q_{ab}}\left[1-\bar{\eta}_0\xi_b P_{ba}\right]+2\Omega\bar{\eta}_0+4\bar{\eta}_0\xi_b\frac{P_{1ba}}{Q_{1ab}}\sqrt{1-\Omega}\\
&\quad+\bar{\rho}\,\bar{\eta}_0\xi_b\bar{K}_b\left(\Omega^2-2\mathrm{i}\Omega\frac{\mathrm{Re}_b}{\xi_b}-\left(\frac{\mathrm{Re}_b}{\xi_b}\right)^2\right)\\
&\quad-\frac{4}{Q_{1ab}}-\bar{\eta}_0\bar{\rho}\frac{\mathrm{Re}_b^2}{\mathrm{We}_b}\left(\frac{1}{\xi_b^2}-1\right)=0,\\
&\frac{(2-\Omega)^2}{Q_{ab}}\left[P_{ab}\xi_a-\bar{\eta}_0\right]+2\Omega-4\xi_a\frac{P_{1ab}}{Q_{1ab}}\sqrt{1-\Omega}\\
&\quad-\bar{\rho}\xi_a\bar{I}_a\left(\Omega^2-2\mathrm{i}\Omega\frac{\mathrm{Re}_a}{\xi_a}-\left(\frac{\mathrm{Re}_a}{\xi_a}\right)^2\right)\\
&\quad+\frac{4}{Q_{1ab}}\bar{\eta}_0+\bar{\rho}\frac{\mathrm{Re}_a^2}{\mathrm{We}_a}\left(\frac{1}{\xi_a^2}-1\right)=0,
\end{aligned}\tag{11}$$

where

$$b=a+h,\quad \xi_r=kr,\quad \xi_{1r}=k_1 r,$$

$$\bar{\eta}_0=\frac{\eta_{01}}{\eta_{02}},\quad \bar{\rho}=\frac{\rho_\mathrm{G}}{\rho_\mathrm{L}},\quad \Omega=\frac{\mathrm{i}\omega}{k^2}\frac{\rho_\mathrm{L}}{\mu},$$

$$\mathrm{Re}_r=\frac{\rho_\mathrm{L}Ur}{\mu},\quad \mathrm{We}_r=\frac{\rho_\mathrm{G}U^2 r}{\sigma},\quad \bar{I}_a=\frac{I_0(ka)}{I_1(ka)},\quad \bar{K}_b=\frac{K_0(kb)}{K_1(kb)},$$

$$P_{r_1,r_2}=P(\xi_{r_1},\xi_{r_2})=I_0(kr_1)K_1(kr_2)+K_0(kr_1)I_1(kr_2),$$

$$Q_{r_1,r_2}=Q(\xi_{r_1},\xi_{r_2})=I_1(kr_1)K_1(kr_2)-K_1(kr_1)I_1(kr_2),$$

$$P_{1r_1,r_2}=P(\xi_{1r_1},\xi_{1r_2}),\quad Q_{1r_1,r_2}=Q(\xi_{1r_1},\xi_{1r_2}).$$

The last mathematical manipulation consists of eliminating the ratio of the initial amplitudes of the perturbation between the two equations of system (11) to end up with the following single equation:

$$\delta_4(k)\Omega^4+\delta_3(k)\Omega^3+\delta_2(k,\Omega)\Omega^2+\delta_1(k,\Omega)\Omega+\delta_0(k,\Omega)=0,\tag{12}$$

where the coefficients δ_i are given in the appendix. This equation, identical to the one developed by Lee and Chen (1991), is the key equation of the problem. It is called the dispersion equation and allows one to calculate the frequency ω of any initial perturbation defined by its wave number k. The resolution of the dispersion equation is not straightforward since the unknown variable and the coefficients are complex. Furthermore, it contains Bessel functions whose arguments are functions of the unknown variable. Therefore, the dispersion equation has to be solved numerically. This was achieved here by using a Newton–Raphson method for non-linear systems. Eq. (12) is decomposed following its real and imaginary parts leading to a system of two equations. Using a first-order Taylor series development for each equation, the system is reduced to a pair of linear equations. An iterative procedure is then used to find the solutions that satisfy both equations at the same time.

Considering the asymptotic case of long wave perturbations ($k\to 0$) applied for a non viscous liquid ($\mu=0$), it can be shown that Eq. (12) reduces to

$$\begin{aligned}
&\omega^4-2kU\omega^3+k^2U^2\left(1+\frac{\beta}{\alpha}\frac{1}{\mathrm{We}_a}\right)\omega^2-\frac{4\sigma Uk^3}{\alpha\rho_\mathrm{L}}\omega\\
&\quad+\frac{U^2\sigma k^4}{\alpha\rho_\mathrm{L}}\left(2+\frac{1}{\mathrm{We}_a}\right)=0,
\end{aligned}\tag{13}$$

where

$$\alpha=\frac{4b^3}{b^2-a^2},\quad \beta=\frac{2(b^3+a^3+a\bar{\rho}(b^2-a^2))}{b^2-a^2}.$$

The resolution of Eq. (13) does not require any numerical development and the solutions of this fourth order equation with real and constant coefficients can be obtained from a commercial mathematical software.

3. Results

The results are presented in a graph $\omega_\mathrm{i}=f(k)$ called the dispersion diagram. As for the case of flat liquid sheets, the dispersion equation is of order 4, leading to two possible growth rates for a single perturbation. As shown by Hagerty and Shea (1955) for the case of flat liquid sheets, these two solutions correspond to the symmetric and antisymmetric modes of perturbation, which differ from the phase difference between the two interfaces. For the antisymmetric mode, this phase difference is zero, whereas for the other mode it is equal to π. These two modes can be differentiated by their respective growth rate, the growth rate of the antisymmetric mode being always higher than that of the symmetric mode. Furthermore, Rangel and Sirignano (1991) showed that the dominance of the antisymmetric mode is always ensured provided that the gas/liquid density ratio is less than 1, which is the case of interest in the present investigation.

Examples of dispersion diagrams are presented in Fig. 2(a) and (b) for the symmetric and the antisymmetric modes of perturbation respectively, and for different relative velocities U. These results were obtained for an annular sheet of water developing in air. The internal radius and the thickness of the sheet were equal to 1 and 0.5 mm, respectively and the viscosity of the liquid was not taken into account.

In order to validate the numerical resolution technique used to solve Eq. (12), the results for the long wave asymptotic case ($k\to 0$) presented in Fig. 2(a) and (b) are compared with the solutions provided by Eq. (13), this latter equation being solved with the software Matlab (version 5.1). The results are presented in Fig. 2(c) and (d) for the symmetric and antisymmetric modes of perturbation respectively. One can observe in these two figures that, for both modes of perturbation, Eqs. (12) and (13) give solutions that show identical slopes at the origin of the dispersion diagram. This result shows the reliable behaviour of the numerical technique used to solve Eq. (12).

The dispersion diagrams presented in Fig. 2(a) and (b) show the expected bell shape, commonly encountered in linear theory analysis. In each situation, a finite range of unstable perturbations, i.e. showing a positive growth rate, is obtained. The maximum wave number of the unstable waves is called the cut-off wave number k_c. The existence of the cut-off wave number has been explained on many different occasions (Squire, 1953, Crapper et al., 1975, Dumouchel and Ledoux, 1991) and results from the stabilising effect of the surface tension forces that increases with the wave number of the imposed perturbation. Another important characteristic of the dispersion diagrams shown in Fig. 2(a) and (b) is the presence of a maximum in any case and whatever the mode of perturbation. This maximum, usually called the dominant wave, is characterised by its wave number k_opt and its growth rate ω_imax. The dominant wave is always considered with a great interest as it is usually assumed that, as this perturbation grows more rapidly than any other, the whole disintegration process is mainly controlled by this perturbation. Therefore, the wave length of the dominant wave is often considered as a characteristic length scale of the atomisation process studied. One can

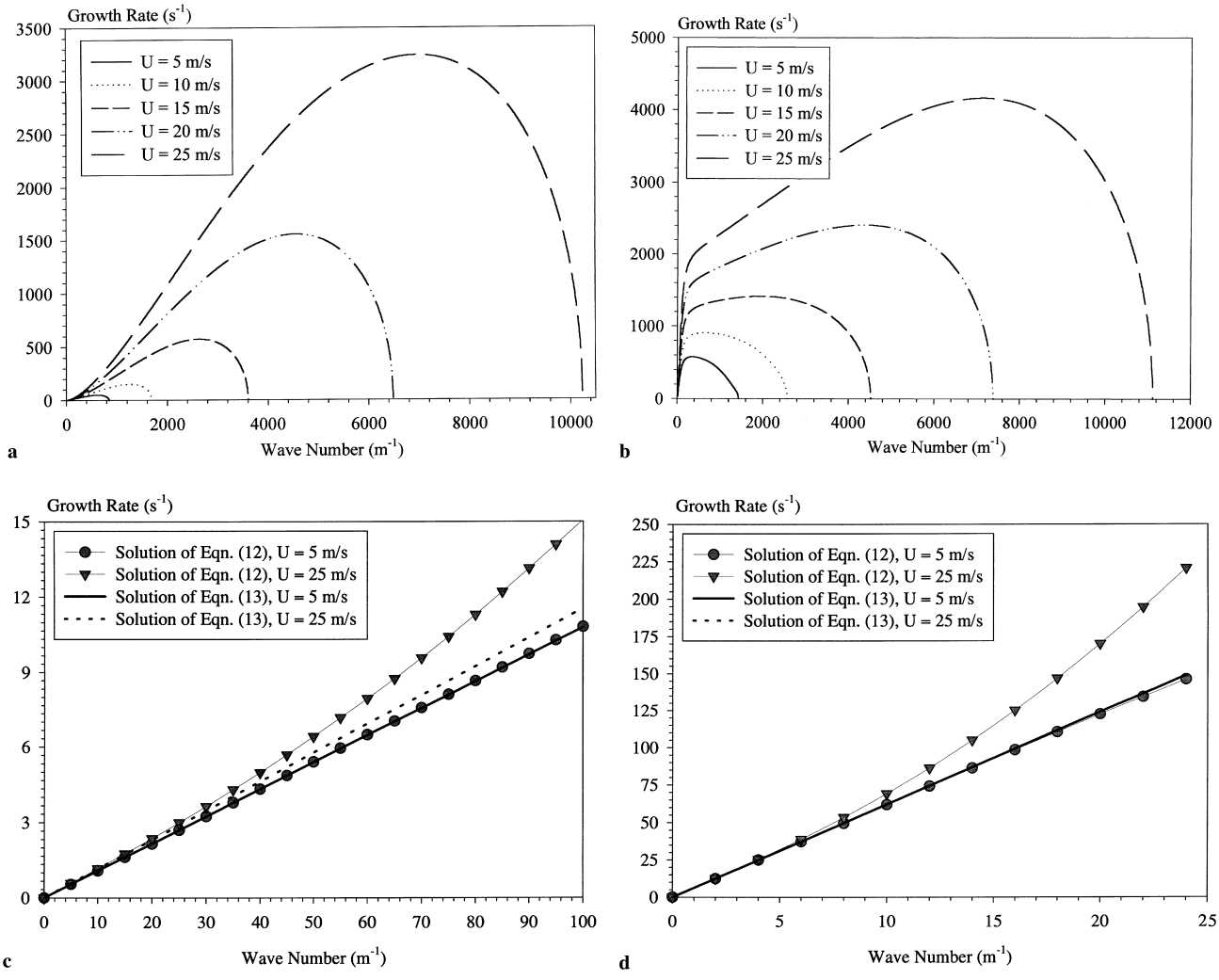

Fig. 2. (a) Dispersion diagram of the symmetric mode of perturbation. (b) Dispersion diagram of the antisymmetric mode of perturbation. (c) Dispersion diagrams for the long wave asymptotic case of the symmetric mode of perturbation. Comparison between Eqs. (12) and (13). (d) Dispersion diagrams for the long wave asymptotic case of the antisymmetric mode of perturbation. Comparison between Eqs. (12) and (13). ($a=1$ mm, $h=0.5$ mm, $\sigma=0.073$ kg s^{-2}, $\rho_G/\rho_L=1.23\times10^{-3}$.)

notice in Fig. 2(a) and (b) that both characteristics of the dominant waves are higher for the antisymmetric mode than for the symmetric mode. Therefore, the growth of an antisymmetric perturbation is likely to be the dominant process. It was decided therefore to concentrate on this mode only within the scope of this work.

Fig. 2(a) and (b) also report the influence of the relative velocity U. As expected, it can be seen that k_c, k_{opt} and ω_{imax} increase as the relative velocity increases. A similar result can be observed when the gas density is increased as it is presented in Fig. 3. This behaviour shows the well-known destabilising effect of the aerodynamic forces that are proportional to $\rho_G U^2$. An increase of these forces leads to an increase of both dominant wave characteristics i.e., it induces a faster disintegration process and the production of smaller drops. The influence reported here is similar to that obtained for a flat liquid sheet (Cousin and Dumouchel, 1996) and has been experimentally observed in many situations. Indeed, it is known that an increase of the liquid injection pressure leads to the production of smaller drops. This shows to which extent the study carried out here can provide physical information on the phenomenon investigated.

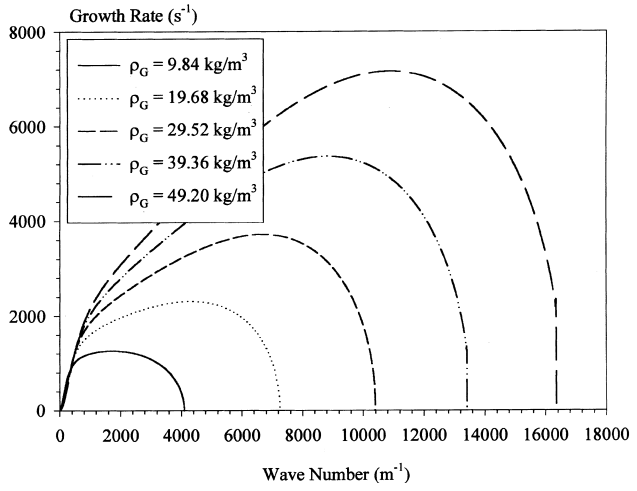

Fig. 3. Dispersion diagram of the antisymmetric mode of perturbation. Influence of the gas density ($a=1$ mm, $h=0.5$ mm, $\sigma=0.073$ kg s^{-2}, $\rho_L=1000$ kg/m^3, $U=5$ m/s).

3.1. Influence of the surface tension

The influence of the surface tension forces on the linear stability of an annular liquid sheet is more complicated than for other liquid systems. As illustrated in Figs. 4 and 5, the influence of the surface tension is a function of the geometry of the annular sheet and, more specifically, of the internal radius of the sheet. Fig. 4 presents the influence of the surface tension on the dispersion diagram of an annular liquid sheet whose internal radius is equal to 10 mm. It can be seen that when the surface tension is increased, both dominant wave characteristics as well as the cut-off wave number decrease. This implies that the disintegration process is getting slower and slower as the surface tension increases and that the diameter of the drops produced increases. This behaviour shows the well-known stabilising effect of the surface tension forces that try to annihilate the perturbation by forcing the interfaces to go back to their initial position. The annular liquid sheet whose behaviour is reported in Fig. 4 behaves as a flat liquid sheet.

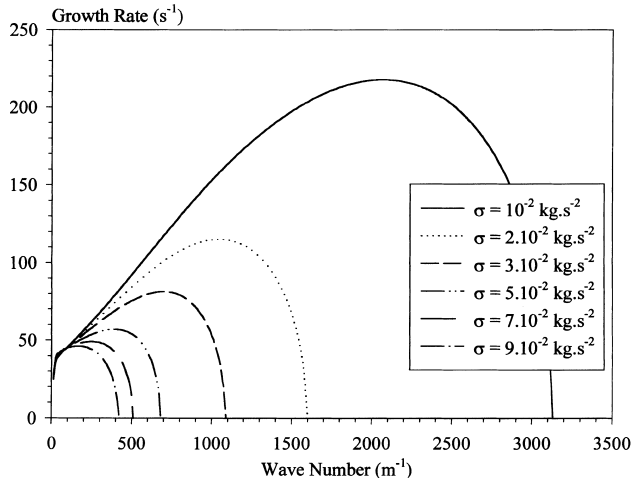

Fig. 4. Effect of the surface tension on the dispersion diagram of the antisymmetric mode of perturbation ($a = 10$ mm, $h = 1$ mm, $U = 5$ m/s, $\rho_G/\rho_L = 1.23 \times 10^{-3}$).

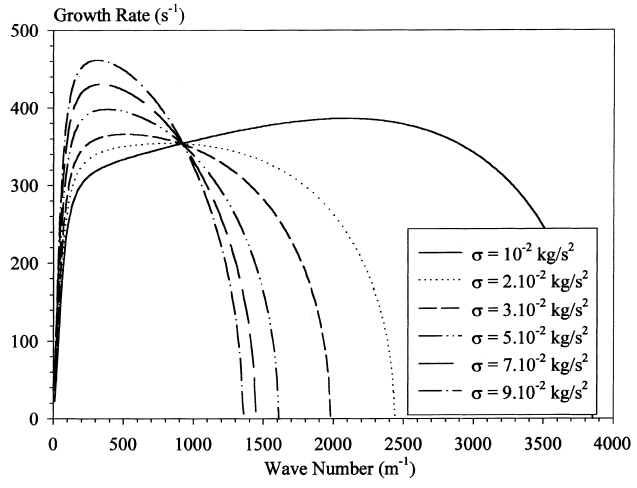

Fig. 5. Effect of the surface tension on the dispersion diagram of the antisymmetric mode of perturbation ($a = 1$ mm, $h = 1$ mm, $U = 5$ m/s, $\rho_G/\rho_L = 1.23 \times 10^{-3}$).

However, when the internal radius of the annular sheet is reduced, the influence of the surface tension is different. This is illustrated in Fig. 5, which shows the influence of the surface tension on the dispersion diagram of the annular liquid sheet whose internal radius has been reduced to 1 mm, the other parameters being kept constant. It can be observed in this figure that the influence of the surface tension is fundamentally different: as σ increases, k_{opt} and k_c decreases as in the first case, but the growth rate of the dominant wave increases. This behaviour can be explained as follows.

Surface tension forces take place when a liquid/gas interface shows a curvature different than zero. For a flat liquid sheet, the curvature of the interfaces results from the presence of the perturbation only. For an annular liquid sheet, the curvature of the interfaces is imposed by the perturbation but also by the natural curvature of the system due to the internal radius. The forces resulting from the presence of the perturbation are stabilising. However, the component related to the internal radius is destabilising and induces an increase of the growth rate when σ increases. This behaviour is identical to the one described by Rayleigh for the case of a low speed cylindrical liquid jet. The double effect of the surface tension can be identified in the expression of $p_{\sigma i}$ (Eq. (10)) that contains two terms. The first one (η/r^2) is the destabilising component of the surface tension forces. For high internal radii, this term is very small and the pressure $p_{\sigma i}$ reduces to the stabilising term and becomes equal to the contribution of the surface tension in the case of a flat sheet. Therefore, in this condition, the annular liquid sheet behaves as a flat liquid system. As found in a previous investigation (Dumouchel and Ledoux, 1991), the condition for an annular liquid sheet to behave as a flat system is related to the Weber number We_a defined by:

$$We_a = \frac{\rho_G U^2 a}{\sigma}. \tag{14}$$

When this number is higher than 10, the surface tension forces introduced by the curvature of the liquid sheet are negligible and the sheet behaves as a flat liquid system.

Finally, it can be noticed in Fig. 5 that when the surface tension increases, the wave number of the dominant wave decreases towards an asymptotic value, i.e., k_{opt} becomes independent of the surface tension. Such behaviour is identical to the one reported by Rayleigh (1879) for the case of cylindrical interfaces destabilised by the action of the surface tension only. For the case reported in Fig. 5, when the surface tension increases, the action of the aerodynamic forces decreases and for the high values of σ, the perturbation growth is likely to be a consequence of the surface tension forces only. Thus, as for the case investigated by Rayleigh, this leads to a constant optimum wave number. This observation shows the good behaviour of the results obtained here and validates also the resolution technique applied on Eq. (12).

Thus, the behaviour of an annular liquid system can be reduced to a simpler system when the internal radius varies. A similar behaviour is found when the thickness of the liquid is varied. When h increases, the two interfaces become independent and the two solutions of Eq. (12) correspond to the solutions of two cylindrical interfaces identical to the one that would be obtained by Weber theory. When h is further increased, the external interface eventually reaches the behaviour of a single flat interface. When this is coupled with a high internal radius a, the annular liquid sheet behaves as two independent flat interfaces and the two solutions are identical. The influence of h on the behaviour of the annular liquid sheet can be related to the Weber number We_h defined by:

$$We_h = \frac{\rho_G U^2 h}{\sigma}. \tag{15}$$

Fig. 6 presents all the asymptotic configurations that can be reached by a non-viscous annular liquid sheet according to the values of We_h and We_a. It is interesting to notice here that the case of a non-viscous annular liquid sheet can be regarded as a very general case from which any classical non-viscous liquid system can be investigated. The classification presented in Fig. 6 may be useful to evaluate the possible influence of the geometrical characteristics h and a on the atomisation process of an annular liquid sheet.

3.2. Influence of the liquid viscosity

The influence of the liquid viscosity on the dispersion diagram of an annular liquid sheet is presented in Fig. 7. These results were obtained for a sheet with an internal radius of 1 mm, a thickness of 500 μm and having a relative velocity with the external medium of 5 m/s. It can be seen in Fig. 7 that when the viscosity increases, both characteristics of the dominant wave decrease. Therefore, the influence of the liquid viscosity is to slow down the disintegration process and to increase the size of the drops. This behaviour is identical to that found for a flat liquid sheet (Cousin and Dumouchel, 1996). It illustrates the stabilising influence of the liquid viscosity observed in many experimental investigations. It is interesting to note in the same figure that the liquid viscosity does not affect the cut-off wave number k_c as for a flat liquid sheet. As illustrated in Fig. 8, which presents the individual contribution of the physical phenomenon on the dispersion diagram, the cut-off wave number is a function of the surface tension forces only. Indeed, when viscosity and surface tension are not taken into account, the dispersion diagram shows no cut-off wave number as the aerodynamic forces can ensure the growth of any sinusoidal perturbation. When the viscosity forces are added, it can be seen that beyond a particular wave number, the growth rate reduces and reaches a constant value as the wave number of the perturbation increases. In this situation also, the dispersion diagram shows no cut-off wave number. A cut-off wave number is obtained only when the surface tension is taken into account, and, as already observed in Fig. 7, the cut-off wave number is not affected by the viscosity of the liquid.

It appears from this investigation that the liquid viscosity may have an important influence on the linear instability of annular liquid sheets. However, this influence is not only a matter of the value of the viscosity but depends also on the other parameters of the system. An example of this is given in Fig. 9, which shows four dispersion diagrams obtained for identical annular liquid sheets except for the values of the viscosity and the velocity. It is interesting to note that the influence of the viscosity is much more important for high relative velocities. It is believed that this behaviour is due to the fact that an increase of the velocity U induces an increase of the perturbation velocity gradients in the liquid i.e. an increase of the viscous forces. Therefore, it was decided to conduct a detailed parametric study in order to discover under which conditions the liquid viscosity has a negligible influence on the linear stability of an annular liquid sheet. This parametric study led us to consider the non-dimensional number D defined by

$$D = \frac{We_h}{Re}\left(We_h + \frac{h}{a}\right). \tag{16}$$

Figs. 10(a) and (b) present the growth rate and wave number of the dominant wave respectively as a function of D. In both figures, the dominant wave characteristics are divided by the

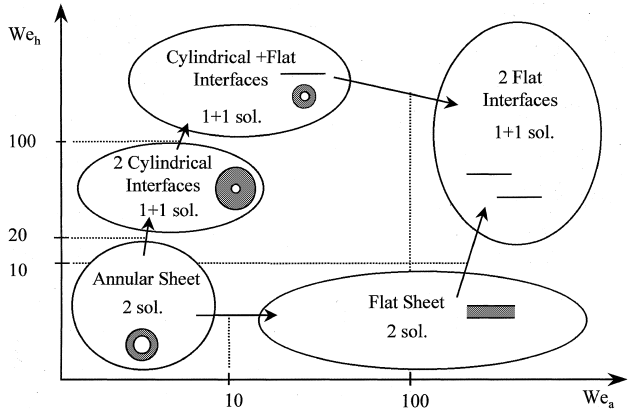

Fig. 6. Asymptotic behaviour and evolution of the two solutions of an annular liquid sheet.

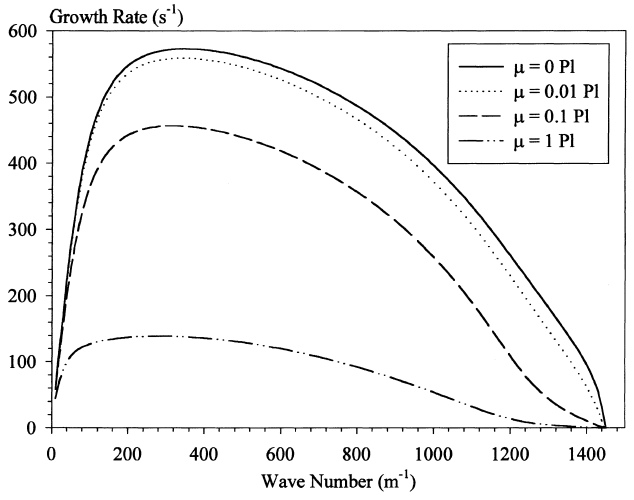

Fig. 7. Effect of the liquid viscosity on the dispersion diagram of the antisymmetric mode of perturbation ($a = 1$ mm, $h = 0.5$ mm, $U = 5$ m/s, $\sigma = 7.3\times10^{-2}$ kg s^{-2}, $\rho_G/\rho_L = 1.23\times10^{-3}$).

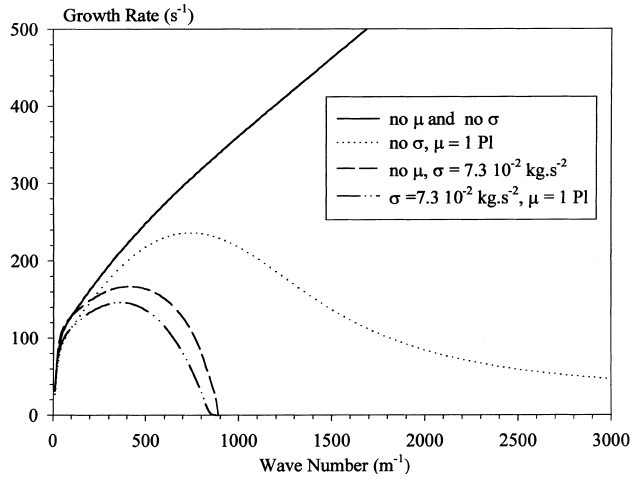

Fig. 8. Contribution of each physical phenomenon on the dispersion diagram of the antisymmetric mode of perturbation ($a = 10$ mm, $h = 1$ mm, $U = 7$ m/s, $\rho_G/\rho_L = 1.23\times10^{-3}$).

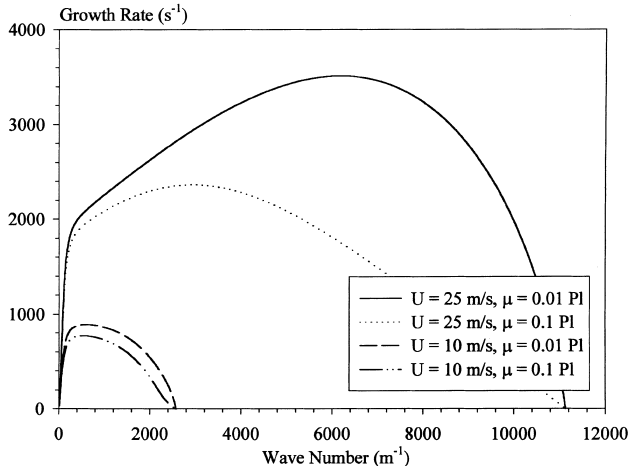

Fig. 9. Influence of the relative velocity on the effect of the liquid viscosity ($a=1$ mm, $h=0.5$ mm, $\sigma=7.3\times10^{-2}$ kg s^{-2}, $\rho_G/\rho_L=1.23\times10^{-3}$).

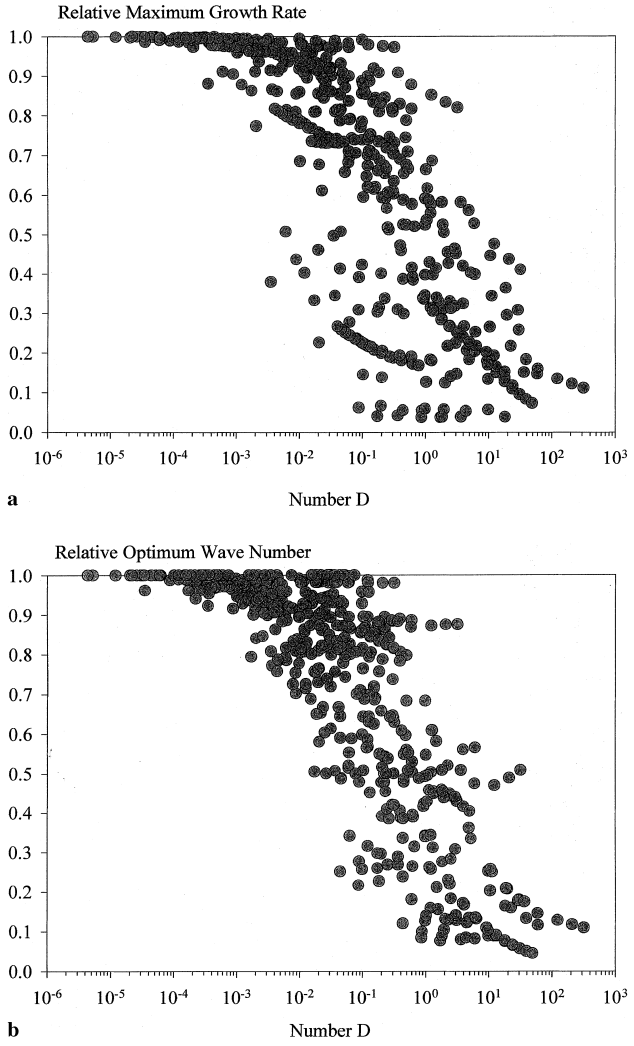

Fig. 10. (a) Relative maximum growth rate versus the number D; (b) relative optimum wave number versus the number D.

values corresponding to the non viscous case. Figs. 10(a) and (b) divide up into two parts. For low $D(<10^{-4})$, the relative dominant wave characteristics remain constant and equal to 1. These values of the parameter D correspond therefore to liquid systems whose stability is not influenced, to first order, by the possible effect of the liquid viscosity.

For $D(>10^{-4})$, both relative growth rate and wave number of the dominant wave show values ranging from 0 to 1, revealing, as observed earlier, a possible decrease of these characteristics because of the liquid viscosity. The parameter D appears as an interesting non-dimensional characteristic of the physics involved in the stability of annular liquid sheets. Furthermore, the parameter D is consistent with the parameter M reported by Cousin and Dumouchel (1996) for the case of a flat sheet. As observed in Fig. 6, an annular liquid sheet adopts the behaviour of a flat liquid sheet when the internal radius is increased. Eq. (16) shows that for a high internal radius, the parameter D reduces to the parameter M.

4. Conclusion

The work reported in this paper can be regarded as an extension of the study carried out by Cousin and Dumouchel (1996) on the flat liquid sheet, by considering the more general case of annular liquid sheets. This implies the consideration of an additional parameter, namely, the internal radius of the sheet. By conducting a linear theory analysis, it has been found that the internal radius introduced additional surface tension forces that increases the growth rate of the perturbation. This surface tension effect that is enhanced as the internal radius of the sheet is reduced, is identical to that observed on a low speed cylindrical jet subjected to the Rayleigh instability. Furthermore, it can be noted from the results reported in the paper that the effect of the surface tension due to the internal radius is more pronounced for small wave number perturbation i.e. for high wave length.

As far as the influence of the viscosity is concerned, the behaviour reported here is similar to that obtained by Cousin and Dumouchel (1996) for a flat liquid system. The viscosity has a clear stabilising effect, reducing the characteristics of the dominant wave, and it has no effect on the cut-off wave number. It was found also that the influence of the viscosity is a function of the other parameters. A non-dimensional group D, consistent with the one obtained by Cousin and Dumouchel (1996), and containing all the physical parameters of the problem, was deduced from a parametric study. This parameter allows one to account for the influence of the viscosity on the stability of an annular liquid sheet.

Finally, the annular liquid system represents an interesting case since it can be regarded as a more general system from which any configuration, ranging from the cylindrical jet to the finite flat interface, can be studied.

Acknowledgements

Part of this work has been carried out within the scope of the European Brite Euram Low NOx III program (contract BR.PR. 95-0122). This work was conducted in the CORIA laboratory within the team of Professor M. Ledoux.

Appendix A

This appendix presents the expressions of the coefficients of the dispersion equation (Eq. (12)):

$$\delta_4(k)=\frac{1}{Q_{ab}^2}\left(\frac{1}{\xi_a\xi_b}-P_{ab}P_{ba}\right)+\frac{\overline{\rho}}{Q_{ab}}\left(P_{ab}\overline{K}_b+P_{ba}\overline{I}_a\right)-\overline{\rho}^2\overline{I}_a\overline{K}_b,$$

$$\begin{aligned}\delta_3(k)=&\frac{-8}{Q_{ab}^2}\left(\frac{1}{\xi_a\xi_b}-P_{ab}P_{ba}\right)-\frac{4\overline{\rho}}{Q_{ab}}\left(P_{ab}\overline{K}_b+P_{ba}\overline{I}_a\right)\\&+2\mathrm{i}\overline{\rho}^2\overline{I}_a\overline{K}_b\left(\frac{\mathrm{Re}_b}{\xi_b}+\frac{\mathrm{Re}_a}{\xi_a}\right)\\&+\frac{2}{Q_{ab}}\left[\frac{P_{ab}}{\xi_b}\left(1-\mathrm{i}\overline{\rho}\overline{K}_b\mathrm{Re}_b\right)-\frac{P_{ba}}{\xi_a}\left(1+\mathrm{i}\overline{\rho}\overline{I}_a\mathrm{Re}_a\right)\right],\end{aligned}$$

$$\begin{aligned}\delta_2(k,\Omega)=&\frac{24}{Q_{ab}^2}\left(\frac{1}{\xi_a\xi_b}-P_{ab}P_{ba}\right)+\frac{4\overline{\rho}}{Q_{ab}}\left(P_{ab}\overline{K}_b+P_{ba}\overline{I}_a\right)\\&+\overline{\rho}\frac{\mathrm{Re}_a^2}{\xi_a}\left(\overline{\rho}\overline{K}_b-\frac{P_{ba}}{Q_{ab}}\right)\left[\frac{\overline{I}_a}{\xi_a}+\frac{1}{\mathrm{We}_a}\left(\frac{1}{\xi_a^2}-1\right)\right]\\&+\overline{\rho}\frac{\mathrm{Re}_b^2}{\xi_b}\left(\overline{\rho}\overline{I}_a-\frac{P_{ab}}{Q_{ab}}\right)\left[\frac{\overline{K}_b}{\xi_b}+\frac{1}{\mathrm{We}_b}\left(\frac{1}{\xi_b^2}-1\right)\right]\\&+\frac{4\sqrt{1-\Omega}}{Q_{1ab}}\left[\frac{P_{1ba}P_{ab}+P_{1ab}P_{ba}}{Q_{ab}}-\overline{\rho}\left(P_{1ba}\overline{I}_a+P_{1ab}\overline{K}_b\right)\right]\\&+\frac{8}{Q_{ab}}\left(\frac{P_{ba}}{\xi_a}-\frac{P_{ab}}{\xi_b}\right)+4\overline{\rho}^2\frac{\mathrm{Re}_a}{\xi_a}\frac{\mathrm{Re}_b}{\xi_b}\overline{I}_a\overline{K}_b\\&+\frac{4}{\xi_a\xi_b}-\frac{8}{Q_{1ab}Q_{ab}\xi_a\xi_b}\\&+4\mathrm{i}\overline{\rho}\left[\mathrm{Re}_a\frac{\overline{I}_a}{\xi_a}\left(2\frac{P_{ba}}{Q_{ab}}+\frac{1}{\xi_b}\right)+\mathrm{Re}_b\frac{\overline{K}_b}{\xi_b}\left(2\frac{P_{ab}}{Q_{ab}}-\frac{1}{\xi_a}\right)\right],\end{aligned}$$

$$\begin{aligned}\delta_1(k,\Omega)=&\frac{-32}{Q_{ab}^2}\left(\frac{1}{\xi_a\xi_b}-P_{ab}P_{ba}\right)+\frac{8}{Q_{ab}}\left(\frac{P_{ab}}{\xi_b}-\frac{P_{ba}}{\xi_a}\right)\\&+\overline{\rho}\frac{\mathrm{Re}_a^2}{\xi_a}\left(\frac{4P_{ba}}{Q_{ab}}-2\mathrm{i}\overline{\rho}\overline{K}_b\frac{\mathrm{Re}_b}{\xi_b}+\frac{2}{\xi_b}\right)\\&\times\left[\frac{\overline{I}_a}{\xi_a}+\frac{1}{\mathrm{We}_a}\left(\frac{1}{\xi_a^2}-1\right)\right]\\&+\overline{\rho}\frac{\mathrm{Re}_b^2}{\xi_b}\left(\frac{4P_{ab}}{Q_{ab}}-2\mathrm{i}\overline{\rho}\overline{I}_a\frac{\mathrm{Re}_a}{\xi_a}-\frac{2}{\xi_a}\right)\\&\times\left[\frac{\overline{K}_b}{\xi_b}+\frac{1}{\mathrm{We}_b}\left(\frac{1}{\xi_b^2}-1\right)\right]\\&-\frac{8\mathrm{i}\overline{\rho}}{Q_{ab}}\left(P_{ba}\overline{I}_a\frac{\mathrm{Re}_a}{\xi_a}+P_{ab}\overline{K}_b\frac{\mathrm{Re}_b}{\xi_b}\right)\\&+\frac{16}{Q_{1ab}\xi_a\xi_b}\left(\frac{2}{Q_{ab}}+\frac{P_{1ab}P_{1ba}}{Q_{1ab}}\right)\\&+\frac{8\sqrt{1-\Omega}}{Q_{1ab}}\left(\frac{P_{1ba}}{\xi_a}\left(1+\mathrm{i}\overline{\rho}\overline{I}_a\mathrm{Re}_a\right)\right.\\&\left.-\frac{P_{1ab}}{\xi_b}\left(1-\mathrm{i}\overline{\rho}\overline{K}_b\mathrm{Re}_b\right)\overline{I}_a\frac{\mathrm{Re}_a}{\xi_a}+P_{ab}\overline{K}_b\frac{\mathrm{Re}_b}{\xi_b}\right)\\&-\frac{16\sqrt{1-\Omega}}{Q_{ab}Q_{1ab}}\left(P_{1ba}P_{ab}+P_{1ab}P_{ba}\right),\end{aligned}$$

$$\begin{aligned}\delta_0(k,\Omega)=&\frac{16}{Q_{ab}^2}\left(\frac{1}{\xi_a\xi_b}-P_{ab}P_{ba}\right)+\frac{16}{Q_{1ab}^2\xi_a\xi_b}\left(1-P_{1ab}P_{1ba}\right)\\&+\frac{16}{Q_{ab}Q_{1ab}}\left[\left(P_{1ba}P_{ab}+P_{1ab}P_{ba}\right)\sqrt{1-\Omega}-\frac{2}{\xi_a\xi_b}\right]\\&+4\overline{\rho}\frac{\mathrm{Re}_a^2}{\xi_a}\left(\frac{P_{1ba}}{Q_{1ab}}\sqrt{1-\Omega}-\frac{P_{ba}}{Q_{ab}}\right)\left[\frac{\overline{I}_a}{\xi_a}+\frac{1}{\mathrm{We}_a}\left(\frac{1}{\xi_a^2}-1\right)\right]\\&+4\overline{\rho}\frac{\mathrm{Re}_b^2}{\xi_b}\left(\frac{P_{1ab}}{Q_{1ab}}\sqrt{1-\Omega}-\frac{P_{ab}}{Q_{ab}}\right)\left[\frac{\overline{K}_b}{\xi_b}+\frac{1}{\mathrm{We}_b}\left(\frac{1}{\xi_b^2}-1\right)\right]\\&-\overline{\rho}^2\frac{\mathrm{Re}_a^2}{\xi_a}\frac{\mathrm{Re}_b^2}{\xi_b}\left[\frac{\overline{I}_a}{\xi_a}+\frac{1}{\mathrm{We}_a}\left(\frac{1}{\xi_a^2}-1\right)\right]\\&\times\left[\frac{\overline{K}_b}{\xi_b}+\frac{1}{\mathrm{We}_b}\left(\frac{1}{\xi_b^2}-1\right)\right].\end{aligned}$$

References

Chigier, N, Dumouchel, C., 1996. Atomization of liquid sheets. In: Kuo, K.K. (Ed.), Recent Advances in Spray Combustion. AIAA1, p. 241.

Cousin, J., Dumouchel, C., 1996. The effect of viscosity on the linear instability of a flat liquid sheet. Atomization and Spray 6, 563–576.

Crapper, G.D., Dombrowski, N., Pyott, G.D., 1975. Kelvin–Helmholtz wave growth on cylindrical liquid sheet. JFM 68, 497–502.

Dumouchel, C., Ledoux, M., 1991. Atomisation of flat and annular liquid sheets practical use of linear theories, paper 12. In: Proceedings of the ICLASS-91, Gaithersburg, MD,USA, pp. 157–164.

Dumouchel, C., Ledoux, M., Bloor, M.I.G., Dombrowski, N., Ingham, D.B., 1990. The design of pressure swirl atomizers. In: 23rd International Symposium on Combustion Institute, pp. 1461–1467.

Hagerty, W.W., Shea, J.F., 1955. A study of the stability of plane liquid sheets. J. Appl. Mech. 509–514.

Lee, J.G., Chen, L.D., 1991. Linear stability analysis of gas–liquid interface. AIAA J. 29 (10), 1589–1595.

Rangel, R.H., Sirignano, W.A., 1991. The linear and nonlinear sheet instability of a fluid sheet. Phys. Fluids A 3 (10), 2392–2400.

Rayleigh, J.W.S., 1879. On the instability of jets. Proc. Lond. Math. Soc. 10, 4–13.

Squire, H.B., 1953. Investigation of the instability of a moving liquid film. Brit. J. Appl. Phys. 4, 167–169.

Sterling, A.M., Sleicher, C.A., 1975. Stability of capillary jets. J. Fluid Mech. 68, 477–495.

Weber, C., 1931. Zum Zerfall eines Flüssigkeitsstrahles. Z. Angew. Math. Mech., 136.

Weihs, D., 1978. Stability of thin, radially moving liquid sheets. JFM 87 (2), 289–298.